Recruitment of cellular prion protein to mitochondrial raft-like microdomains contributes to apoptosis execution

Vincenzo Mattei[a,*], Paola Matarrese[b,c,*], Tina Garofalo[d], Antonella Tinari[e], Lucrezia Gambardella[b], Laura Ciarlo[b], Valeria Manganelli[d], Vincenzo Tasciotti[a], Roberta Misasi[d], Walter Malorni[b,f,†], and Maurizio Sorice[d,†]

[a]Laboratory of Experimental Medicine and Environmental Pathology, Sabina Universitas, 02100 Rieti, Italy; [b]Section of Cell Aging and Degeneration, Department of Therapeutic Research and Medicine Evaluation, Istituto Superiore di Sanità, 00161 Rome, Italy; [c]Center of Integrated Metabolomics, 00161 Rome, Italy; [d]Department of Experimental Medicine, "Sapienza" University, 00161 Rome, Italy; [e]Department of Technology and Health, Istituto Superiore di Sanità, 00161 Rome, Italy; [f]San Raffaele Institute Sulmona, 67039 L'Aquila, Italy

ABSTRACT We examined the possibility that cellular prion protein (PrP[C]) plays a role in the receptor-mediated apoptotic pathway. We first found that CD95/Fas triggering induced a redistribution of PrP[C] to the mitochondria of T lymphoblastoid CEM cells via a mechanism that brings into play microtubular network integrity and function. In particular, we demonstrated that PrP[C] was redistributed to raft-like microdomains at the mitochondrial membrane, as well as at endoplasmic reticulum-mitochondria–associated membranes. Our in vitro experiments also demonstrated that, although PrP[C] had such an effect on mitochondria, it induced the loss of mitochondrial membrane potential and cytochrome c release only after a contained rise of calcium concentration. Finally, the involvement of PrP[C] in apoptosis execution was also analyzed in PrP[C]-small interfering RNA–transfected cells, which were found to be significantly less susceptible to CD95/Fas–induced apoptosis. Taken together, these results suggest that PrP[C] might play a role in the complex multimolecular signaling associated with CD95/Fas receptor–mediated apoptosis.

INTRODUCTION

Prions are infectious pathogens that cause a group of invariably fatal neurodegenerative diseases mediated by a novel mechanism. Prion disease is seemingly due to the conversion of a normal cell surface glycoprotein (PrP[C]) into a conformationally altered isoform (PrP[Sc]) that is infectious in the absence of nucleic acid. Microvesicle release has been suggested to contribute to the intercellular mechanism of PrP diffusion and prion spread (Mattei et al., 2009). Hence both PrP[Sc] and PrP[C] have been intensively investigated, although their intracellular activity is poorly understood (Prusiner, 1998). Several studies suggested that PrP[C] is involved in the regulation of presynaptic copper concentration, intracellular calcium homeostasis, lymphocyte activation, astrocyte proliferation, and cellular resistance to oxidative stress (Bounhar et al., 2001; Watt et al., 2005; Hu et al., 2008). Moreover, recent studies show the involvement of PrP[C] in apoptotic signaling pathways (Chiesa et al., 2005; Zhang et al., 2006). Apoptosis is a highly conserved and essential feature of development and homeostasis in higher organisms. Progress has been made in identifying extracellular, intracellular, and cell surface molecules that regulate apoptosis (Ayllon et al., 2002). Of note, two different apoptotic pathways have been described: receptor-mediated apoptosis and mitochondrial-mediated apoptosis. The first comes from receptor triggering, for example, in cells expressing CD95/Fas at their surface; the second

comes from a direct mitochondria-mediated series of events. It has been suggested that either PrP^{Sc} or PrP^C can actively participate in the regulation of apoptosis. In particular, Roucou et al. (2005) showed that PrP^{Sc} prevents Bax-mediated cell death by inhibiting the conformational changes of this proapoptotic protein. This was observed in human primary neurons and in epithelial cells as due to a still unknown mechanism. Other authors, investigating how PrP^C could regulate cell fate, found apparently conflicting results. In particular, Hachiya et al. (2005) showed that transgenic mice harboring a high copy number of wild-type mouse PrP^C developed a spontaneous neurological dysfunction probably due to mito-chondria-mediated neuronal apoptosis in aged transgenic mice overexpressing wild-type PrP^C. The aged mice exhibited an aberrant mitochondrial localization of PrP^C concomitant with decreased manganese superoxide dismutase activity, cytochrome c release, caspase-3 activation, and DNA fragmentation, most predominantly in hippocampal neuronal cells. However, more recently, a protective function of PrP^C has been hypothesized in T lymphocytes under oxidative stress (Aude-Garcia et al., 2011). In general, literature data seem to suggest that PrP^C could exert a protective role in mitochondria-mediated apoptosis, for example, due to mitochondrially targeted drugs (Choi et al., 2007).

Localization of proteins to distinct subcellular compartments, including membranes, is a critical event in multiple cellular pathways, such as apoptotic one. Plasma membranes of different cell types contain microdomains, commonly referred to as lipid rafts (Simons and Ikonen, 1997). These domains are enriched in sphingolipids and cholesterol. In T cells, a number of proteins involved in signal transduction pathways copurify with lipid rafts isolated on a sucrose gradient (Anderson et al., 2000; Langlet et al., 2000). Like other glycosylphosphatidylinositol (GPI)-anchored proteins, most PrP^C molecules are found in lipid rafts from neural and nonneural cells (Vey et al., 1996; Masserini et al., 1999; Naslavsky et al., 1999). In addition, sphingolipid-rich rafts play an essential role in the post-translational formation of PrP^{Sc} from its normal conformer PrP^C (Borchelt et al., 1990; Taraboulos et al., 1995).

With this in mind, we evaluated the possible role of PrP^C in the modulation of the physiological apoptotic stimulus in T cells, that is, the receptor-mediated apoptotic signaling pathway. In this regard, the role of PrP^C in CD95/Fas–induced apoptosis, taking into account the role of microdomains, was considered. We found that, in T lymphoblastoid cells, upon CD95/Fas ligation, a clear redistribution of PrP^C from the plasma membrane microdomains to the mitochondrial rafts occurred, and this relocalization was crucial for apoptosis execution.

RESULTS

Evidence for PrP^C–MitoTracker colocalization following CD95/Fas treatment

We analyzed the distribution of PrP^C in untreated and anti-CD95/Fas–treated lymphoblastoid CEM cells (Figure 1A). The immunofluorescence analysis, performed by intensified video microscopy (IVM) and confocal microscopy, clearly indicated a preferential plasma membrane localization of PrP^C in control samples (Figure 1A, top row), as previously demonstrated (DeMarco and Dogget, 2009). In contrast, an evident relocalization of PrP^C to the mitochondrial compartment was detectable in anti-Fas–treated cells (as revealed by yellow staining in the merge picture of Figure 1A, second row). Two different experimental controls were performed in order to confirm the specificity of this redistribution: the first deals with GM1, a marker known to colocalize with PrP^C at the plasma membrane (Mattei et al., 2002), and the second with CD71, the transfer-

rin receptor, a plasma membrane PrP^C-unrelated marker. We found that after anti–CD95/Fas treatment, the association GM1/PrP^C at the cell surface was decreased (Supplemental Figure S1), whereas no overlapping fluorescence CD71/mitochondria was detected (Supplemental Figure S2), indicating that in our experimental conditions the transferrin receptor localization was unaffected by proapoptotic stimulation.

The morphometric analysis (Figure 1B, left) also underlined that PrP^C/mitochondria association occurred in a time-dependent manner, starting 30 min after anti-Fas administration and reaching a peak 1 h after CD95 engagement. As expected, the percentage of apoptotic cells after Fas triggering increased with time (Figure 1B, right). The redistribution of PrP^C after CD95 engagement was partially inhibited by pretreatment with the intracellular Ca^{2+} chelator 1,2-bis(o-aminophenoxy)ethane-N,N,N′,N′-tetraacetic acid (BAPTA) (Figure 1A, third row, and Figure 1B, left). In the same vein, cell pretreatment with methyl-β-cyclodextrin (MβCD), which alters lipid raft organization, significantly prevented the anti-Fas–induced relocalization of PrP^C at mitochondrial level (Figure 1A, bottom row, and Figure 1B, left). Of importance, either BAPTA or MβCD significantly inhibited anti-Fas–induced apoptosis as well (Figure 1B, right). Of note, the "increase" of apoptosis in cells pretreated with MβCD for 2 h is lower than that observed in cells without MβCD. This means that MβCD was able to partially prevent Fas-triggered cell apoptosis.
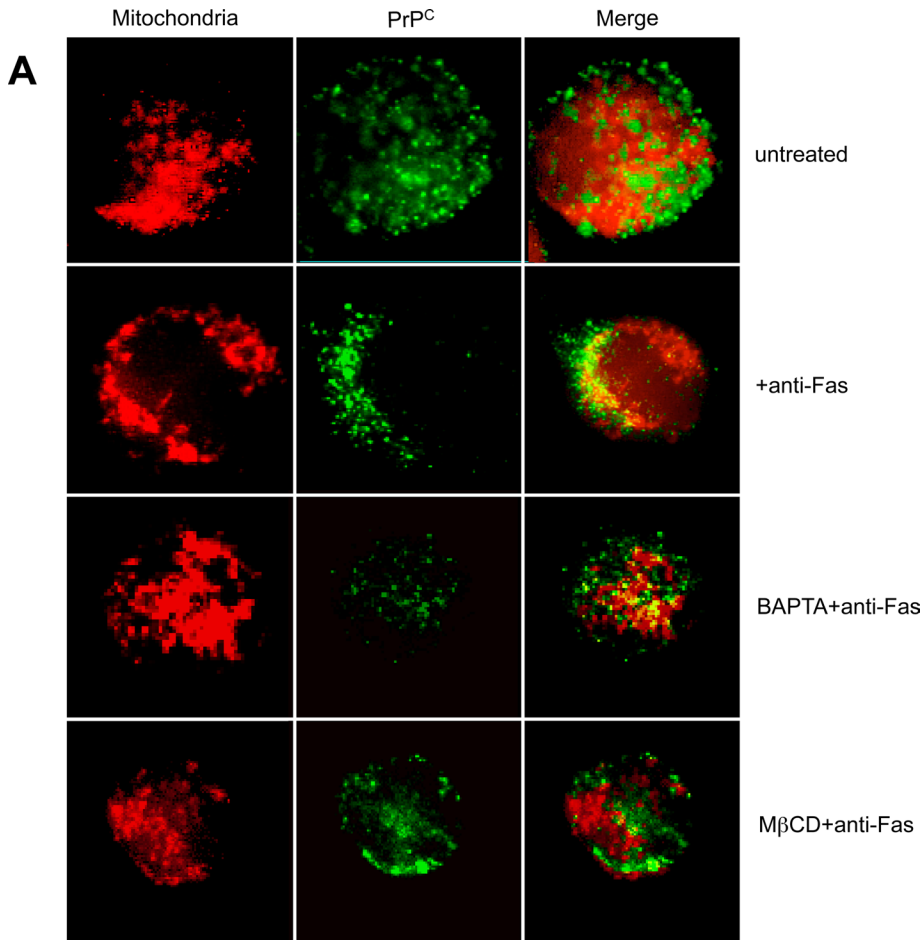
PrP^C redistribution in continuous sucrose density gradient fractions following CD95/Fas treatment

On the basis of these morphological observations, which could imply a directional movement of PrP^C toward mitochondrial compartment, we decided to analyze in detail the subcellular distribution of PrP^C in our system, that is, following anti–CD95/Fas triggering. Experiments were thus performed to analyze PrP^C distribution by Western blotting, by means of cell subfractionation after a continuous 10–40% sucrose density gradient. PrP^C, which was concentrated in the high-density fractions in untreated cells (Figure 2), where a typical plasma membrane marker (CD71, transferrin receptor) is enriched, moved to fractions with lower density 1 h after anti–CD95/Fas treatment. Of interest, we observed a redistribution of PrP^C toward the voltage-dependent, anion-selective channel protein-1 (VDAC-1)–enriched fractions, corresponding to mitochondria-enriched fractions, following CD95/Fas triggering.

Evidence for the presence of PrP^C in crude mitochondria preparations following anti–CD95/Fas treatment

Crude mitochondria preparations were subjected to 12% SDS–PAGE. Western blot analysis revealed a 33-kDa positive band, detected by anti-PrP monoclonal antibody (mAb; SAF 32) in samples treated with anti–CD95/Fas (250 ng/ml for 1 h at 37°C; Figure 3A). As expected, no bands were detectable from untreated cells.

Next, we evaluated the association of PrP^C with GD3, considered as a prototypical ganglioside component of raft-like microdomains in mitochondria (Garofalo et al., 2005), by coimmunoprecipitation experiments. Acidic glycosphingolipids, extracted from the PrP^C immunoprecipitates either untreated or treated with anti–CD95/Fas (250 ng/ml for 1 h at 37°C), were immunostained by a high selective anti-GD3 mAb. The results indicate that PrP^C strictly interacts with GD3 in cells treated with anti–CD95/Fas (250 ng/ml for 1 h at 37°C) but not in untreated cells (Figure 3B). The immunoprecipitate was revealed as PrP^C, as detected by Western blot, using the anti-PrP mAb (6H4). Under the same experimental conditions, the immunoprecipitation with immunoglobulin G (IgG) did

FIGURE 1: Evidence for PrP^C–MitoTracker colocalization following CD95/Fas treatment. (A) IVM analysis after double cell staining with MitoTracker Red/PrP shows that PrP^C colocalized with mitochondria in anti-CD95/Fas–treated cells only. The yellow fluorescence areas observed in the merge picture indicate the colocalization. (B) Left, morphometric analyses indicate a time-dependent effect of anti-Fas in inducing mitochondria/PrP^C colocalization. The ordinate represents the percentage of cells in which yellow fluorescence was detected. Right, the percentages of annexin V–positive cells in different experimental conditions. Statistical analysis indicates a significant (p < 0.01) decrease of mitochondria/PrP^C colocalization and Fas-induced apoptosis in cells pretreated either with BAPTA or MβCD. Data are reported as mean ± SD of the results obtained in three independent experiments.

not result in detectable levels of PrP^C (Figure 3C). The purity of the mitochondrial preparations was assessed by Western blot by checking subunit IV of cytochrome *c* oxidase (COX-IV), lysosome-associated membrane glycoprotein (LAMP-1), transferrin receptor (CD71), and the endoplasmic reticulum (ER)/mitochondria-associated membrane (MAM)–associated glycoprotein calnexin (Figure 3D). Our analysis revealed the presence of COX-IV and calnexin but not of the other markers. This suggests that our preparation also contains MAM (Wieckowski *et al.*, 2009; Gilady *et al.*, 2010).

Next we complemented these data by analyzing by flow cytometry the levels of PrP^C in mitochondria from untreated or anti-Fas–treated CEM cells. As illustrated in Figure 3E, mitochondria from untreated CEM cells showed a very low expression of PrP^C (left, solid, light gray histogram, and right, gray column). Treatment with anti-Fas for 1 h significantly (p < 0.01) increased the levels of PrP^C associated with mitochondria (left, open black histogram, and right, black column). As a positive control the expression of VDAC-1 was analyzed (Figure 3E, left, solid, dark gray histogram).

Evidence for the presence of PrP^C in both MAM and isolated mitochondria following anti–CD95/Fas treatment

To better clarify the distribution of PrP following anti–CD95/Fas triggering, we performed an immuno–electron microscopy analysis using the anti-PrP mAb. It revealed that the protein is present mainly on mitochondrial membrane, but also in ER-MAM (Figure 4A). After subcellular fractionation, mitochondria and MAM were isolated and analyzed separately by Western blot. Our analysis confirmed that, following CD95/Fas triggering, PrP^C was present on mitochondrial membrane as well as in MAM (Figure 4B). The purity of the subcellular preparations was assessed by Western blot by checking COX-IV and calnexin, respectively (data not shown).

Effect of human recombinant PrP on mitochondria

The next step was to verify whether mitochondria could represent a direct target of PrP^C. We investigated the ability of human recombinant PrP 23-230 (rec PrP) to induce swelling in mitochondria obtained from CEM cells. First, to test the vitality of mitochondria, we added 300 μM calcium to the mitochondria preparation to induce a rapid loss of mitochondrial membrane potential. Figure 5A (top row) shows a representative profile of
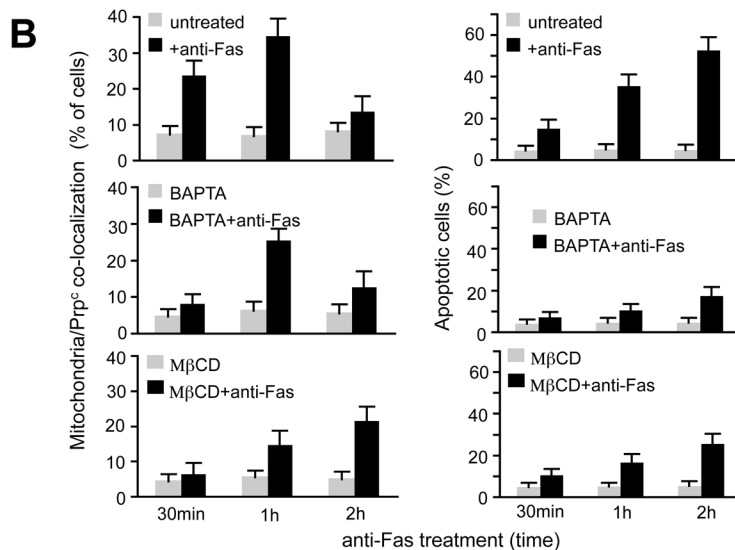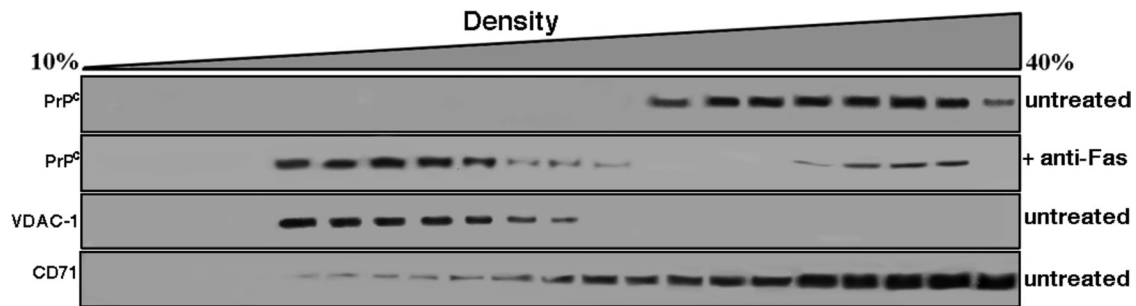
FIGURE 2: PrP^C redistribution in continuous sucrose density gradient fractions following CD95/Fas treatment. CEM cells, either untreated or treated with anti–CD95/Fas (250 ng/ml for 30 min at 37°C), were lysed in lysis buffer, and postnuclear supernatant was prepared and loaded on top of a continuous 10–40% (wt/vol) sucrose gradient. After centrifugation, fractions were collected, separated by SDS–PAGE, and analyzed by Western blot. Fractions obtained after sucrose density gradient centrifugation, either untreated or treated with anti–CD95/Fas (250 ng/ml) cells, were analyzed using anti-PrP mAb (SAF 32). As controls, fractions obtained after sucrose density gradient centrifugation from untreated cells were analyzed using a polyclonal anti–VDAC-1 or a monoclonal anti-CD71.

the mitochondrial swelling induced by 300 μM calcium monitored by means of the variations in tetramethylrhodamine-methyl-ester-perchlorate (TMRM) fluorescence as a function of time. We also verified that 10 μM calcium was ineffective in itself to induce mitochondrial alterations. The analysis of the mitochondria swelling profile pointed to a dose-dependent effect of rec PrP in inducing the increase of mitochondrial membrane potential (i.e., hyperpolarization). In fact, as shown in Figure 5A (second row), rec PrP provoked an increase in the percentage of mitochondria with increased membrane potential (i.e., hyperpolarized) starting from a concentration of 0.1 μg/ml.

Of interest, rec PrP was able to induce the loss of mitochondrial membrane potential after 10 μM Ca^{2+} addition only, indicating an important role for calcium in the rec PrP–induced effects on mitochondria (Figure 5A, third row). Of importance, the addition of 10 μM calcium chloride did not induce in itself any sign of mitochondrial swelling, although it was indispensable for the PrP^C-induced mitochondrial membrane depolarization (Figure 5A, top row). This result is in accord with the effects induced by the calcium chelator BAPTA on Fas-induced apoptosis shown in Figure 1. In light of this, we also investigated the role of Ca^{2+} in modulating the ability of rec PrP to induce the release of cytochrome c (cyt C) from mitochondria purified from CEM cells. These results were obtained by analyzing the supernatants of swelling experiments (before TMRM staining) by means of an enzyme-linked immunosorbent assay (ELISA). Figure 5B shows that 1) 300 μM calcium chloride induced the release of a significant amount of cyt C, 2) 10 μM Ca^{2+} alone was ineffective in inducing cyt C release, and 3) rec PrP induced the release of cyt C only in the presence of 10 μM Ca^{2+}. As a control, we demonstrated that rec PrP, when added to crude mitochondria preparation, interacts with mitochondria (Figure 5C).

Taken together, these data clearly indicate that rec PrP exerted a direct effect on mitochondria, which was improved by a contained rise in calcium concentration. As expected, the release of cyt C was strictly associated with the loss of mitochondria membrane potential (i.e., depolarization).

Cytoskeleton integrity as a prerequisite for PrP^C trafficking
On the basis of previous work supporting the key role of microtubular network integrity in raft component trafficking throughout the cell cytoplasm (Sorice et al., 2009), we investigated whether the microtubular network could play a role in PrP^C redistribution after CD95/Fas engagement. To evaluate whether microtubular network integrity could play a role in this PrP^C redistribution, specific immu-

nofluorescence time-course analyses were carried out in cells treated with anti–CD95/Fas in the presence or absence of the microtubule polymerization inhibitor demecolcine (DMC). The results obtained by performing a double labeling of PrP^C and tubulin clearly indicated that early after CD95 engagement (30 min) PrP^C/tubulin colocalization was detectable in a significant percentage of anti-Fas–treated cells (Figure 6A, second row). This percentage decreased 1 and 2 h after CD95/Fas triggering (Figure 6B, left). In cells treated with DMC before anti-Fas administration, the colocalization PrP^C/tubulin was inhibited, as demonstrated by the reduction of yellow staining (Figure 6A, fourth row, see merge picture, and Figure 6B, left). Finally, the analysis of the apoptotic rate by flow cytometry evaluation of annexin V binding (Figure 6B, right) demonstrated that DMC, at least at the low concentration used in these experiments (0.1 μg/ml), 1) was not cytotoxic per se (apoptosis <7%), 2) impaired PrP^C traffic, and 3) reduced CD95/Fas–triggered cell death.

Taken together, our data suggest that 1) microtubular network integrity is required for the redistribution of PrP^C to the mitochondrial compartment following CD95/Fas triggering and 2) PrP^C relocalization at the mitochondrial level plays a role in CD95/Fas–triggered apoptosis of CEM cells.

Effect of PrP^C small interfering RNA on PrP^C–tubulin association and apoptosis
To evaluate the role of PrP^C as a regulator of apoptosis, a small interfering RNA (siRNA) was used for knock down of PrP^C and its function. Cytofluorimetric analyses of siRNA-treated cells revealed that PrP^C expression appeared to be significantly reduced as compared with control cells (Figure 7A, right). Optimum transfection efficiency, confirmed by positive control siGLO laminin A/C siRNA with fluorescent label, was ~65% (Figure 7A, left).

The cytofluorimetric analysis of CD95/Fas–induced apoptosis revealed a significant impairment of CD95/Fas–triggered apoptosis in PrP^C siRNA–transfected cells as compared with cells transfected with nonsilencing siRNA (Figure 7B).

Functional role of PrP^C in HeLa cells
To confirm our results in a different CD95/Fas–sensitive cell line, crude mitochondria preparations from HeLa cells were separated by SDS–PAGE and analyzed by Western blot. Our results confirmed the presence of PrP^C band in samples obtained from cells treated with anti–CD95/Fas (250 ng/ml for 1 h at 37°C) but not in those obtained from untreated cells (Figure 8A).
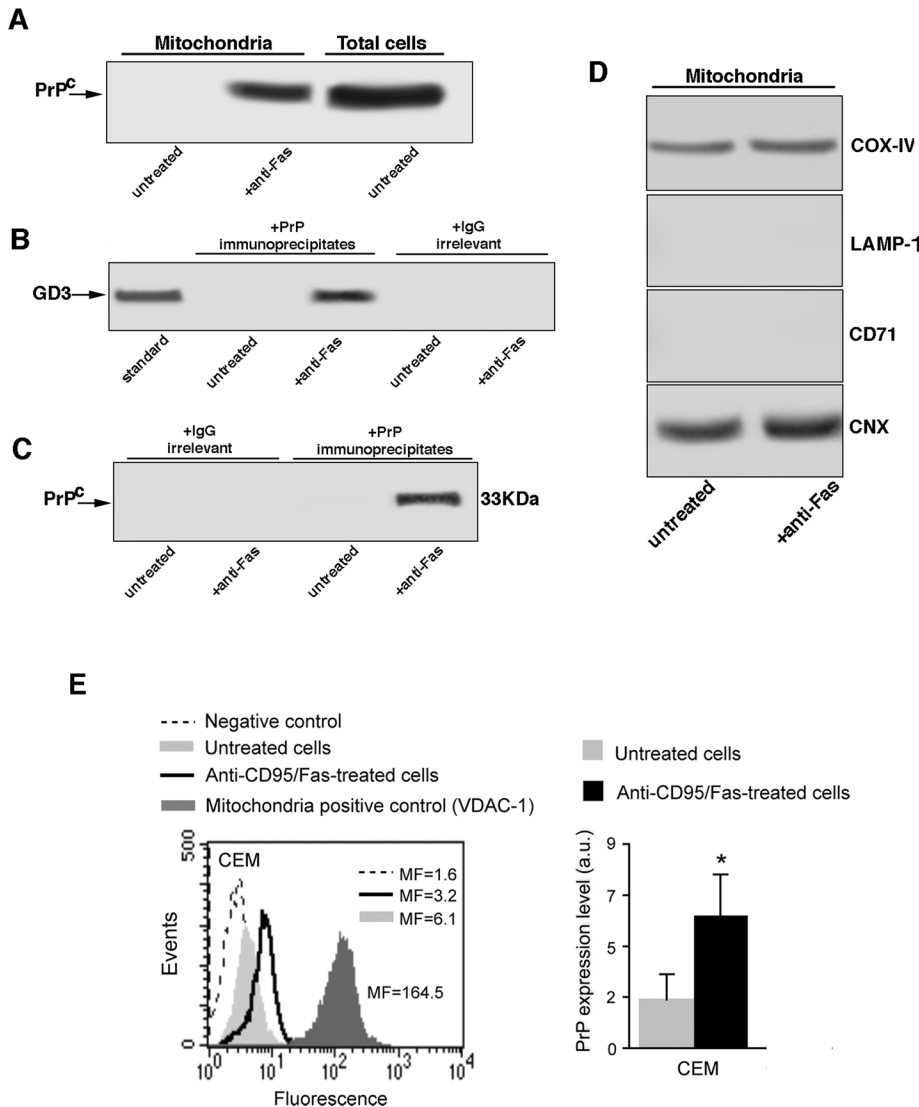
FIGURE 3: Evidence for the presence of PrP^C in crude mitochondria preparation following anti–CD95/Fas treatment. (A) Crude mitochondria preparations from CEM cells, either untreated or treated with anti–CD95/Fas, were obtained from CEM cells by standard differential centrifugation according to Zamzami et al. (2001) and analyzed by Western blot. PrP^C localization was detected using an anti-PrP mAb (SAF 32). (B) Crude mitochondria preparations from CEM cells, either untreated or treated with anti–CD95/Fas, were lysed in lysis buffer, followed by immunoprecipitation with anti-PrP mAb (SAF 32). A mouse IgG isotypic control was used. The immunoprecipitates were subjected to ganglioside extraction. The extracts were run on HPTLC aluminum-backed silica gel and were analyzed for the presence of GD3, using an anti-GD3 MoAb (GMR19). (C) As a control, the immunoprecipitates were assessed by immunoblot with anti-PrP mAb (6H4). (D) The purity of the mitochondrial preparations was checked by Western blot using specific mAbs against COX-IV, LAMP-1, transferrin receptor (CD71), or calnexin. The same amounts of proteins for each sample were run. (E) Cytofluorimetric analysis of PrP^C in crude mitochondria preparations. Left, results obtained in a representative experiment performed in mitochondria obtained from untreated (solid, light gray histograms) or anti–CD95/Fas–treated cells (open, black histograms). The negative control (IgG1 plus anti–mouse Alexa 488) is represented by the dashed curves. The positive control (anti–VDAC-1 plus anti–mouse Alexa 488) is represented by the solid, dark gray histogram. Numbers represent the median values of fluorescence intensity histograms. Right, mean ± SD of the results obtained from three independent experiments. Statistical analysis by Student's *t* test indicated a significant (p < 0.01) increase of the amount of PrP^C after anti–CD95/Fas administration.

Then we investigated the ability of rec PrP to induce swelling in mitochondria obtained from HeLa cells. The analysis of mitochondria swelling profile pointed to a dose-dependent effect of rec PrP in in-

ducing the increase of mitochondrial membrane potential (i.e. hyperpolarization; Figure 8B). Again, rec PrP was able to induce the loss of mitochondrial membrane potential after addition of 10 μM Ca^{2+}. Of note, this effect was more evident than in T cells, confirming an important role for calcium in the rec PrP–induced effects on mitochondria.

To evaluate the role of PrP^C in HeLa cells, siRNA was used for knock down of PrP^C and its function. Again, cytofluorimetric analyses of siRNA-treated cells revealed that PrP^C expression appeared to be significantly reduced as compared with control cells (Figure 8C).

The cytofluorimetric analysis of CD95/Fas–induced apoptosis revealed a significant impairment of CD95/Fas–triggered apoptosis in PrP^C siRNA–transfected HeLa cells as compared with cells transfected with nonsilencing siRNA, as revealed by annexin V/propidium iodide staining (Figure 8D).

DISCUSSION

Evidence for the involvement of lipid rafts in the localization and trafficking of PrP^C, as well as in PrP^C-mediated cellular signaling, has recently been reported in neuronal and nonneuronal cells (Mattei et al., 2002, Mattei et al., 2004; Lewis and Hooper, 2011). Lipid rafts, defined as cholesterol- and glycosphingolipid-enriched plasma membrane microdomains, are implicated in several signal transduction pathways, including CD95/Fas–triggered apoptosis in T cells (Garofalo et al., 2003). This may be due to the recruitment of tumor necrosis factor–family receptors, as well as CD95/Fas, to lipid rafts following receptor engagement (Hueber et al., 2002). In addition, in the apoptotic cascade, the recruitment of lipid raft components, mainly GD3, to the mitochondria has also been suggested (García-Ruiz et al., 2000, 2002; Garofalo et al., 2005). In this context, the present work 1) indicates that PrP^C redistributes to ER-MAM following CD95/Fas treatment; 2) identifies PrP^C as a new component of mitochondrial raft-like microdomains in cells undergoing CD95/Fas–mediated apoptosis; and 3) suggests that microtubular network integrity and function could play a role in the redistribution of PrP^C to the mitochondria.

The recruitment of PrP^C within mitochondrion-associated raft-like microdomains following CD95/Fas triggering is quite surprising, although the involvement of lipid rafts in the localization and trafficking of PrP^C and in the cellular signaling has already been reported (Lewis and Hooper, 2011). Usually, PrP^C is anchored at the cell surface via a GPI moiety (Stahl et al., 1987). However, this protein has also been found associated with many intracellular compartments.
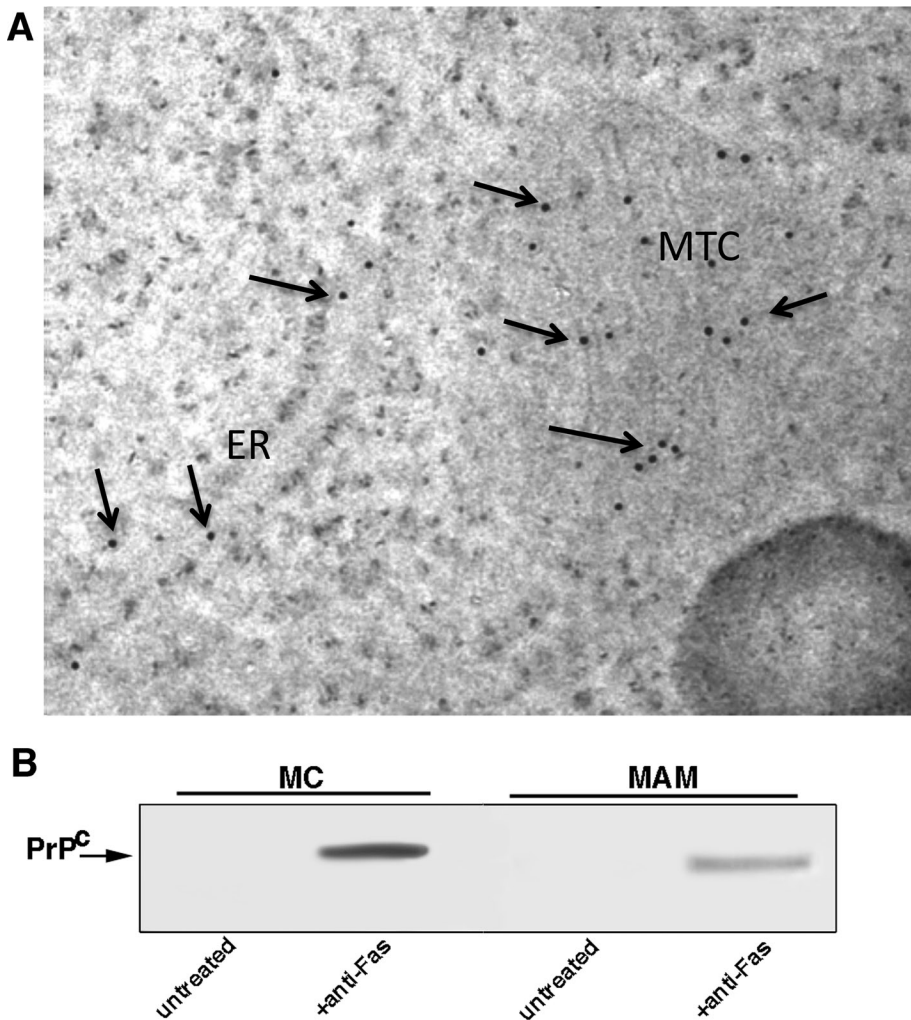
FIGURE 4: Evidence for the presence of PrP^C in mitochondria and MAM following anti–CD95/Fas treatment. (A) PrP^C distribution in mitochondria and MAM following CD95/Fas treatment. Immunogold labeling of PrP^C as detectable on thin sections by transmission electron microscopy by using a postembedding technique (Ciarlo *et al.* 2010). Note that gold particles (arrows) are visible either on mitochondria (MTC) or on endoplasmic reticulum (ER). (B) PrP^C distribution in high-purity MAM and mitochondria fractions following CD95/Fas treatment. Crude mitochondria preparations obtained from cells either untreated or treated with anti–CD95/Fas were subjected to Percoll gradient fractionation. After centrifugation, high-purity MAM and mitochondria fractions were obtained and analyzed by Western blot. PrP^C localization was detected using an anti-PrP mAb (SAF 32).

direct interaction between PrP^C and tubulin was already reported (Nieznanski *et al.*, 2005). In particular, recent evidence demonstrated that PrP^C can associate with different cytoskeletal components, such as actin, α-actinin, and tubulin (Nieznanski *et al.*, 2005; Petrakis and Sklaviadis, 2006). It was suggested that, during apoptosis, microtubules may be used as tracks to direct intracytoplasmic transport of the glycosphingolipid microdomains toward the mitochondria (Sorice *et al.*, 2009). We hypothesize that in cells under CD95/Fas proapoptotic stimulation the cytoplasmic trafficking of PrP^C could be carried out via cytoskeletal elements by using a nonacidic compartment bound by cholesterol-rich membranes (Garofalo *et al.*, 2007). Of interest, the PrP^C/cytoskeleton association was detected even in blood platelets, where it was found significantly increased following their activation (Brouckova and Holada, 2009). This is particularly interesting in relation to the fact that immunological activation of platelets was reported to be associated with mitochondria hyperpolarization (Matarrese *et al.*, 2009), which was also detected in the present study (see later discussion).

Indeed, scrambling among different cell organelles, including plasma membrane, ER, and MAM, as well as lysosomal vesicles and Golgi apparatus, was also hypothesized after triggering of death receptors (Degli Esposti *et al.*, 2009). For instance, the importance of ER in the apoptotic cascade has recently been investigated (Csordas *et al.*, 2006; Faitova *et al.*, 2006). Under ER stress, ER transmembrane receptors initiate the unfolded protein response (Lai *et al.*, 2007). If the adaptive response fails, apoptotic cell death ensues. This response is associated with organelle remodeling and intermixing and is implicated in the pathophysiology of several neurodegenerative and cardiovascular diseases (Szegezdi *et al.*, 2006). Furthermore, the possible implication of Golgi apparatus remodeling in apoptosis execution was also analyzed in detail (Siegel *et al.*, 2004). We suggest that lipid microdomains could have a role in this traffic, participating in structural and biochemical remodeling and leading to carrying out of the cell death program. In particular, lipid rafts may be involved in a series of functions, such as 1) the recruitment of proteins to the mitochondria, including molecules associated with mitochondrial fission (Ciarlo *et al.*, 2010); 2) oxidative phosphorylation and ATP production (Jin *et al.*, 2011); and, finally, 3) the redistribution of mitochondria in discrete regions of the cell cytoplasm (Sorice *et al.*, 2011), thus contributing to cell remodeling and polarization. In line with these observations, our data seem to suggest that, upon apoptotic stimulation, PrP^C could undergo intracellular relocalization to mitochondrion-associated microdomains via MAM and the microtubular network.

The possible role of PrP^C in apoptosis is strongly supported by the effect of recombinant PrP on mitochondria. The analysis of the

In fact, evidence revealed the association of PrP^C with lipid microdomains at the ER (Campana *et al.*, 2006), as well as with the cytoskeleton network (Mironov *et al.*, 2003). Because the ER-MAM represents a subcompartment of the ER connected to the mitochondria and displays the characteristics of lipid rafts (Hayashi and Fujimoto, 2010; Williamson *et al.*, 2011), we investigated whether PrP^C may be present in this compartment. Our IM observations revealed that PrP^C was actually present in both MAM and mitochondrial membranes. Moreover, when we analyzed the PrP^C intracytoplasmic trafficking in CD95/Fas–treated cells, we found that the microtubular network–perturbing agent DMC impaired either mitochondrial relocalization of PrP^C or apoptosis induction. Hence we hypothesize that microtubules could play key roles in the intracellular directional redistribution of PrP^C, as well as in the recruitment of this small polypeptide to the mitochondrial compartment following CD95/Fas triggering. The involvement of microtubules in PrP^C traffic was not surprising since a
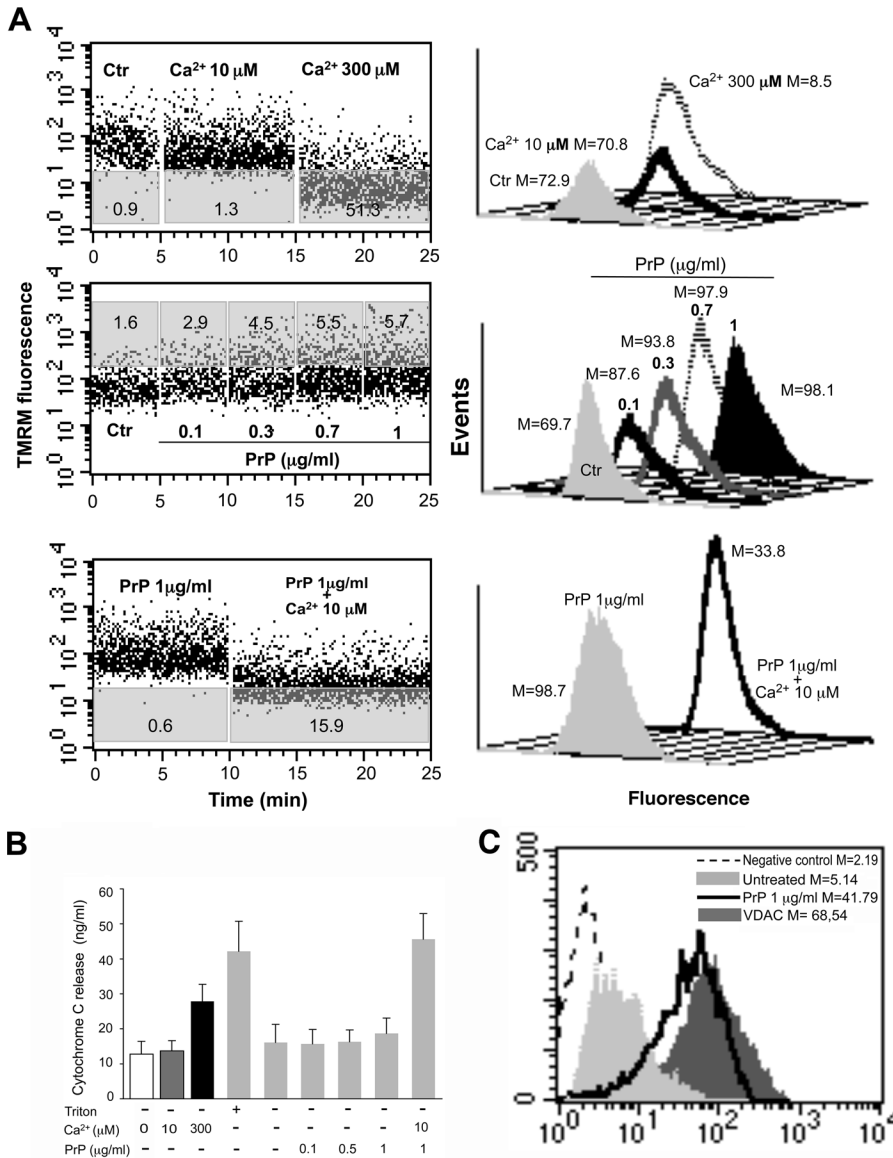
FIGURE 5: Effect of recombinant PrP on mitochondria. (A) Swelling induction in mitochondria. Left, the swelling profile of mitochondria obtained from untreated CEM cells as monitored by means of variations in TMRM fluorescence as a function of time. Numbers in gray areas of each plot represent the percentage of mitochondria that underwent MMP increase (middle dot plot) or decrease (top and bottom dot plots). Results obtained in a representative experiment are shown. Note that 1) 300 μM calcium used as positive control induced a rapid loss of mitochondrial membrane potential, whereas calcium 10 μM was ineffective (top dot plot), 2) recombinant PrP was able to induce dose-dependent mitochondrial membrane hyperpolarization (middle dot plot), and 3) the supplement of 10 μM calcium after the PrP administration provoked a decrease of MMP in a significant percentage of cells (bottom dot plot). Right, analysis of MMP after TMRM staining of living isolated mitochondria in different experimental conditions. Numbers represent the median fluorescence values. (B) Quantitative evaluation of cytochrome c release in the supernatant of isolated mitochondria as revealed by ELISA. Note the effect of 10 μM Ca^{2+} in addition to recombinant PrP on the cytochrome c release. (C) Cytofluorimetric analysis of PrP^C in crude mitochondria preparations. Left, results obtained in a representative experiment performed in mitochondria obtained from untreated cells (solid, light gray histograms) and rec PrP–treated cells (black histograms). The negative control (IgG1 plus anti–mouse Alexa 488) is represented by the dashed curves. The positive control (anti-VDAC-1 plus anti–mouse Alexa 488) is represented by the solid, dark gray histogram. Numbers represent the median values of fluorescence intensity histograms. Right, the mean ± SD of the results obtained from three independent experiments.

mitochondria swelling profile pointed to a dose-dependent effect of PrP^C in inducing the increase of mitochondrial membrane potential (i.e., hyperpolarization), followed by the "typical" loss of mitochon-

dria membrane potential (i.e., depolarization) and the release of apoptogenic factors, such as cytochrome c. Of note, our results also suggest a key role for calcium in the PrP-induced effects on mitochondria. Because mitochondrial microdomains have been suggested to participate in mitochondrial alterations occurring during apoptosis (Garofalo et al., 2005; Malorni et al., 2007; Ziolkowski et al., 2010), we cannot rule out the possibility that PrP^C could play a further role in the morphogenic changes occurring to this organelle, for example, fission processes. This hypothesis is corroborated by the observation that silencing PrP^C protein by siRNA resulted in a significant reduction of CD95/Fas–triggered apoptosis of cells.

In conclusion, although contradictory evidence on the role of PrP^C in the apoptotic process has been published (Roucou et al., 2005; Zhang et al., 2006; Anantharam et al., 2008), our results support the view of a proapoptotic role of PrP^C or, at least, its association with the apoptosis execution program. In this regard, our findings prompted us to hypothesize two levels of regulation of cell apoptosis by PrP^C: on microtubules, where an early interaction of PrP^C with tubulin can alter microtubule framework integrity (Li et al., 2011), and, later, on the mitochondrial membrane, where it interacts with raft-like microdomains. Finally, since PrP^C raft-mediated trafficking appears to strictly depend upon apoptotic triggering, we can also suggest a reappraisal of the previously hypothesized formation of PrP^{Sc} within acidic compartments. In fact, it seems conceivable that once apoptotic stimulation triggers lipid raft–mediated signaling, lipid rafts could contribute to define the metabolic fate of PrP^C. In other words, if raft-embedded PrP^C is part of the complex framework normally contributing to the death of the cell, a defective trafficking of PrP^C from and toward lipid rafts could also represent a sort of "risk factor" or favor an alteration of normal PrP^C catabolism, also leading to the formation of the 17-kDa polypeptide hydrolysis to form the PrP 27-30 scrapie isoform.

MATERIALS AND METHODS
Cells and treatments
Human lymphoblastoid CEM cells (Foley et al., 1965) and HeLa cells were maintained in RPMI 1640 (Invitrogen Italia, Milan, Italy) or DMEM (both Life Technologies-BRL, Life Technologies Italia, Milan, Italy), respectively, containing 10% fetal calf serum plus 100 U/ml penicillin and 10 mg/ml streptomycin at 37°C in humidified CO_2 atmosphere. For apoptosis induction, cells were stimulated with anti–CD95/Fas immunoglobulin M (IgM) mAb (clone CH11; Upstate Biotechnology, Lake Placid, NY) at
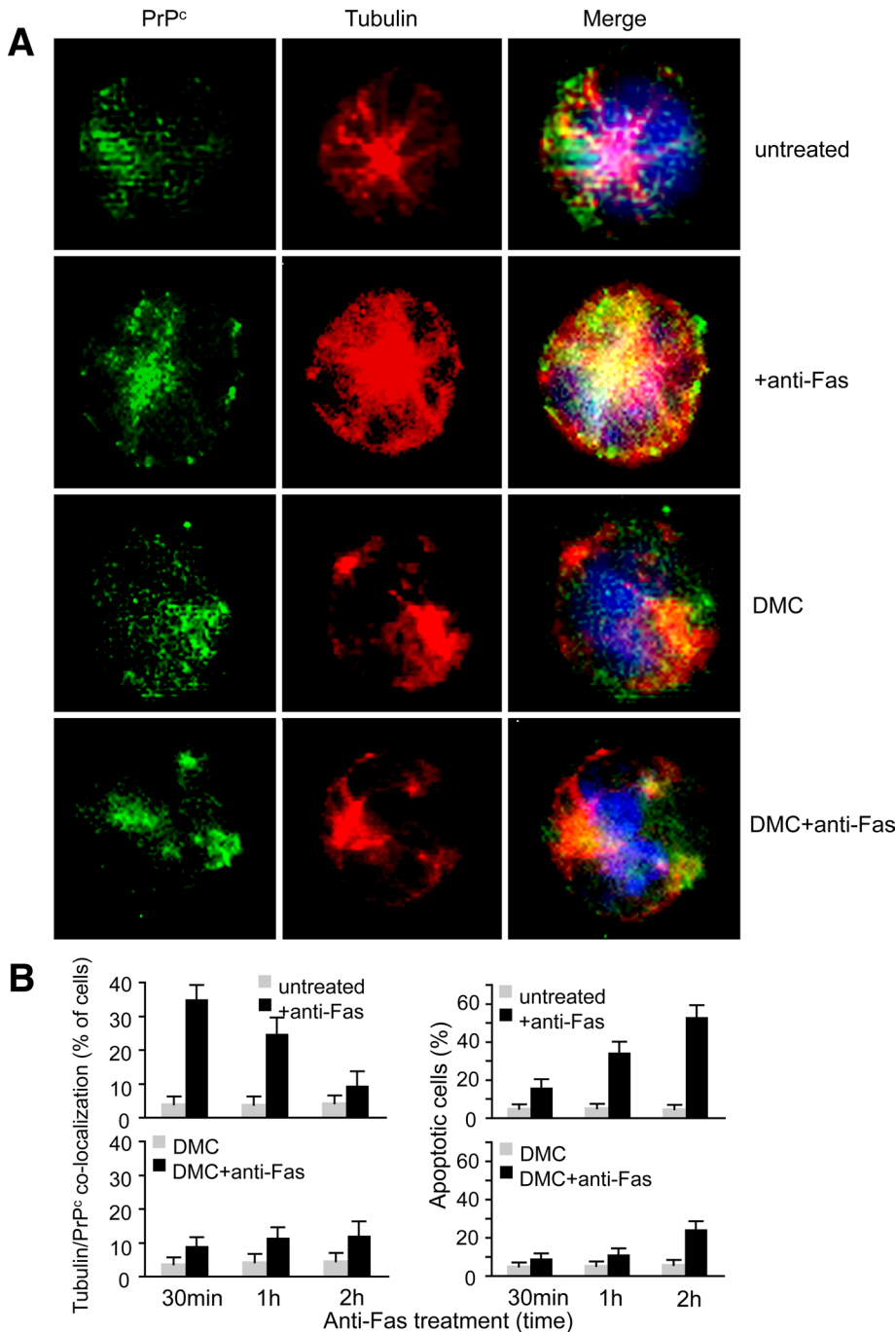
FIGURE 6: Cytoskeleton integrity as a prerequisite for PrP^C trafficking. (A) IVM analysis after double cell staining with PrP^C (green) and tubulin (red) shows that PrP^C colocalized with tubulin very early (30 min) after Fas triggering. The yellow fluorescence areas observed in the merge picture indicate the colocalization. Pretreatment with DMC before anti-Fas administration prevented tubulin/PrP^C colocalization (fourth row). (B) Left, morphometric analyses indicate a time-dependent effect of anti-Fas in inducing tubulin/PrP^C colocalization. The ordinate represents the percentage of cells in which yellow fluorescence was detected. Right, the percentages of annexin V–positive cells in different experimental conditions. Statistical analysis indicates a significant ($p < 0.01$) decrease of tubulin/PrP^C colocalization and Fas-induced apoptosis in cells pretreated with a nontoxic concentration of DMC. Data are reported as mean ± SD of the results obtained in three independent experiments.

St. Louis, MO); or 3) 0.2 μg/ml DMC (Sigma-Aldrich). For swelling experiments, isolated mitochondria were stimulated with rec PrP (Alicon, Schlieren, Switzerland) at different concentration (0.1, 0.3, 0.7, 1 μg/ml) for 20 min.

Immunofluorescence by intensified video microscopy

Control and treated cells were stained with 1 mM MitoTracker Red (Molecular Probes) After washing in phosphate-buffered saline (PBS), cells were fixed with 4% paraformaldehyde in PBS for 30 min at room temperature and then permeabilized with 0.5% Triton X-100 in PBS for 5 min at room temperature, as previously reported (Malorni et al., 2008). Alternatively, lymphoblastoid cells were incubated for 45 min for polyclonal antibody anti-tubulin (Santa Cruz Biotechnology, Santa Cruz, CA), followed by addition of Alexa Fluor 594–conjugated anti–rabbit IgG (Molecular Probes). After three washes in PBS, samples were incubated with anti-PrP mAb (SAF 32; SPI Bio, Montigny Le Bretonneux, France) for 1 h at 4°C, followed by addition (30 min at 4°C) of Alexa Fluor 488–conjugated anti–mouse IgG (Molecular Probes). After washing, cells were counterstained with Hoechst 33258 and then suspended in glycerol/PBS (pH 7.4) and observed with a Nikon (Melville, NY) Microphot fluorescence microscope. Images were captured by a color-chilled 3CCD camera (Hamamatsu, Hamamatsu, Japan) and analyzed by OPTILAB software (Graftek, Paris, France).

Morphometric analyses

Evaluation of the percentage of cells with mitochondria/PrP^C or tubulin/PrP^C colocalization was performed by analyzing double color fluorescence images. At least 200 cells for each experimental point were counted. Only those cells in which mitochondria/PrP^C overlapping was observed (characterized by yellow fluorescence) were considered in our analysis.

Sucrose gradient fractionation

Analysis of the distribution of PrP^C was performed by centrifugation on a continuous density gradient, as previously described (Stockinger et al., 2002). Briefly, ~1.5 × 10^8 CEM cells, either untreated or treated with anti–CD95/Fas (250 ng/ml for 30 min at 37°C), were resuspended in 0.3 ml of buffer (3 mM imidazole, pH 7.4, 1 mM EDTA, and a 1:100 [vol/vol] cocktail of protease inhibitors) containing 8.5% sucrose. The cell suspension was mechanically disrupted by Dounce homogenization (20 strokes), and the efficiency was monitored by microscopy (Olympus Italia, Segrate, Milan, Italy). Nuclei

250 ng/ml for the indicated incubation times at 37°C. In some experiments, before anti-Fas administration, cells were treated for 20 min with 1) the intracellular calcium chelator BAPTA (10 μM; Molecular Probes, Eugene, OR); 2) 2 mM MβCD (Sigma-Aldrich,
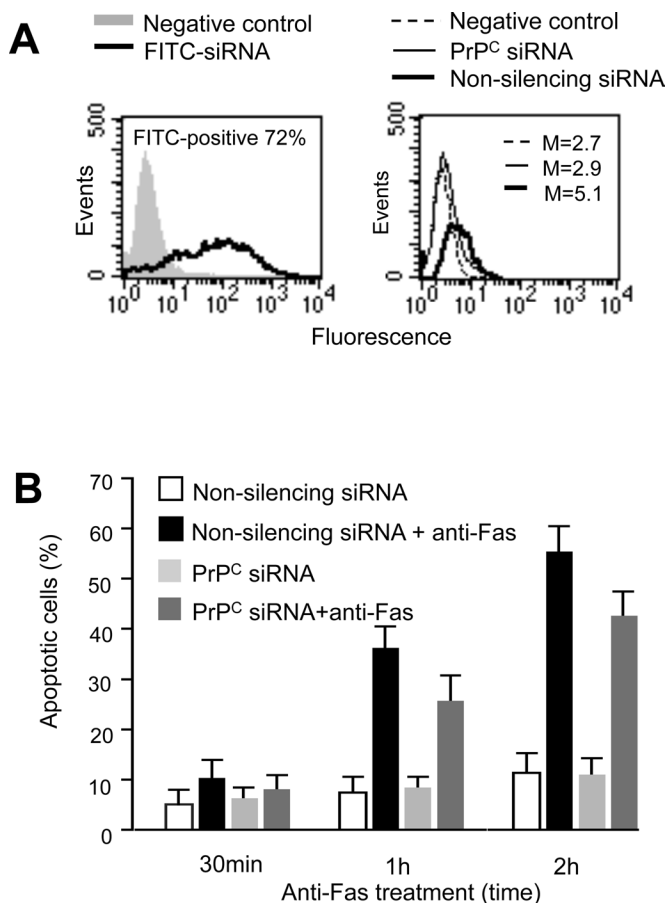
FIGURE 7: Effect of PrP^C siRNA on PrP^C–tubulin association and apoptosis. (A) Left, cytofluorimetric analysis of fluorescence emission in CEM cells transfected with FITC-siRNA. The percentage of FITC-positive cells was considered indicative of the transfection efficiency. The number represents the percentage of FITC-positive cells (corresponding to transfected cells). Right, cytofluorimetric evaluation of PrP^C expression 72 h after siRNA transfection. The numbers represent the median fluorescence intensity and indicate the expression level of PrP^C. A representative experiment among three is shown. (B) Bar graphs showing quantitative cytofluorimetric analysis of apoptosis after cell staining with annexin V–FITC/propidium iodide. Values reported represent the percentage ± SD of positive cells obtained from three different experiments.

were removed by 10 min of centrifugation at 1000 × *g*, and the supernatant was loaded on top of 4 ml of a 10–40% continuous sucrose gradient and centrifuged at 40,000 rpm for 16 h at 4°C in a SW60Ti rotor (Beckman Instruments, Palo Alto, CA). After centrifugation, the gradient was fractionated, and 20 fractions were collected from the bottom of the tube by puncturing with an 18-gauge needle. All steps were carried out at 0–4°C. After evaluation of the protein concentration by Bradford Dye Reagent assay (Bio-Rad, Richmond, CA) samples were analyzed by Western blotting using the anti-PrP mAb (SAF 32; SPI Bio).

Immuno–electron microscopy

Thin sections, collected on gold grids, were treated with PBS containing 1% (wt/vol) gelatin, 1% BSA, 5% fetal calf serum, and 0.05% Tween 20 and then incubated with anti-PrP mAb (SAF 32) and diluted 1:10 in the same buffer without gelatin overnight at 4°C. After washing for 1 h at room temperature, sections were labeled with

protein A–10-nm gold conjugate (1:10) for 1 h at room temperature and washed again. Negative controls were incubated with the gold conjugate alone.

Crude mitochondria preparation

Cells were harvested by a solution containing 0.25% (wt/vol) trypsin and 0.02% (w/v) EDTA in a calcium- and magnesium-free PBS solution and collected by centrifugation. After three washing in PBS, cells were resuspended in homo-buffer (10 mM 4-(2-hydroxyethyl)-1-piperazineethanesulfonic acid [HEPES], pH 7.4, 1 mM ethylene glycol-bis(-aminoethyl ether) N,N',N'-tetraacetic acid [EGTA], 0.1 M sucrose, 5% bovine serum albumin [BSA], 1 mM phenylmethylsulfonyl fluoride [PMSF], and complete protease inhibitor cocktail) and maintained for 10 min on ice. After this time, cells were homogenized with ~50 strokes of a Teflon homogenizer with B-type pestle as previously reported (Zamzami *et al.*, 2001) for 10 min at 4°C to remove intact cells and nuclei, and the supernatants were further centrifuged at 10,000 × *g* at 4°C for 10 min to precipitate the heavy membrane fractions (enriched in mitochondria). These fractions were then purified by standard differential centrifugation. The mitochondrial pellet obtained was resuspended in swelling buffer (SB) containing 0.1 M sucrose, 0.5 M sodium succinate, 50 mM EGTA at pH 7.4, 1 mM phosphoric acid (H_3PO_4), 0.5 M 3[*N*-morpholino] butane-sulfonic acid, and 2 mM rotenone, kept on ice, and used within 2 h from the preparation.

The purity of crude mitochondria preparation was assessed by Western blot by checking LAMP-1, transferrin receptor (CD71), subunit IV of cytochrome *c* oxidase (COX-IV), and calnexin (p88, IP90), using specific mAbs (anti–LAMP-1, BD PharMingen, San Diego, CA; anti-CD71, BD PharMingen; anti-COX-IV, Molecular Probes) and rabbit anti-calnexin (Sigma-Aldrich).

Fractionation of crude mitochondria

Crude mitochondria obtained from cells, either untreated or treated with anti–CD95/Fas, were fractionated to isolate high-purity MAM and mitochondria fractions according to Wieckowski *et al.* (2009). Briefly, crude mitochondrial pellet was resuspended in 2 ml of ice-cold mitochondria resuspending buffer (MRB) containing 250 mM mannitol, 5 mM HEPES (pH 7.4), and 0.5 mM EGTA and loaded on top of 8 ml of Percoll medium (225 mM mannitol, 25 mM HEPES, pH 7.4, 1 mM EGTA, and 30% Percoll [vol/vol]) in an ultracentrifuge tube. Afterward, the tube was gently filled up with 3.5 ml of MRB solution and centrifuged at 95,000 × *g* for 30 min at 4°C in an SW 41 rotor (Beckman). After centrifugation, a dense band containing purified mitochondria was localized approximately at the bottom, whereas MAM fraction was visible as diffuse white band located above the mitochondria. The fractions were collected and centrifuged at 6300 × *g* for 10 min at 4°C. MAM supernatant was subjected to a further centrifugation at 100,000 × *g* for 1 h at 4°C in a 70-Ti rotor (Beckman). After evaluation of the protein concentration by Bradford Dye Reagent assay (Bio-Rad), both MAM and mitochondria fractions were analyzed by Western blot analysis using the anti-PrP mAb (SAF 32) (SPI Bio), as described next.

Western blot analysis of crude mitochondria preparations

Crude mitochondria preparations obtained from CEM or HeLa cells, either untreated or treated with anti–CD95/Fas, were subjected to 12% SDS–PAGE. The proteins were electrophoretically transferred onto nitrocellulose membrane (Bio-Rad) and then, after blocking with PBS containing 3% milk, probed with anti-PrP mAb (SAF 32; SPI Bio). Bound antibodies were visualized with horseradish peroxidase (HRP)–conjugated anti–mouse IgG (Amersham Biosciences,
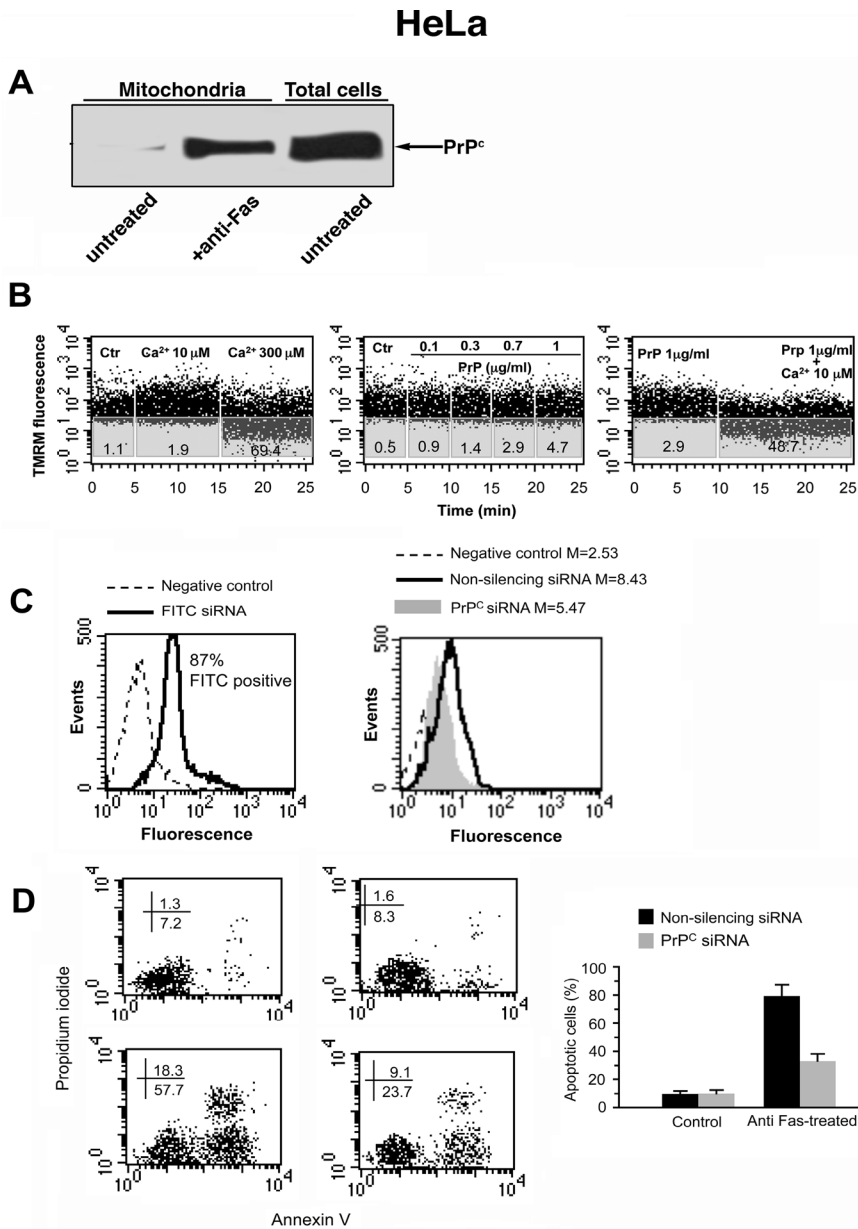
HeLa

FIGURE 8: Functional role of PrP^C in HeLa cells. (A) Crude mitochondria preparations from HeLa cells either untreated or treated with anti–CD95/Fas were obtained from HeLa cells by standard differential centrifugation and analyzed by Western blot. PrP^C localization was detected using an anti-PrP mAb (SAF 32). (B) Swelling induction in mitochondria. The swelling profile of mitochondria obtained from untreated HeLa cells as monitored by means of variations in TMRM fluorescence as a function of time. Results obtained in a representative experiment are shown. Note that 1) 300 μM calcium used as positive control induced a rapid loss of mitochondrial membrane potential, whereas calcium 10 μM was ineffective (left dot plot), 2) rec PrP was able to induce dose-dependent mitochondrial membrane hyperpolarization (middle dot plot), and 3) the supplement of 10 μM calcium after the PrP administration provoked a decrease of MMP in a significant percentage of cells (right dot plot). (C) Left, cytofluorimetric analysis of fluorescence emission in HeLa cells transfected with FITC-siRNA. The percentage of FITC-positive cells was considered indicative of the transfection efficiency. The number represents the percentage of FITC-positive cells (corresponding to transfected cells). Right, cytofluorimetric evaluation of PrP^C expression 72 h after siRNA transfection. The numbers represent the median fluorescence intensity and indicate the expression level of PrP^C. A representative experiment among three is shown. (D) Cytofluorimetric analysis of nonsilencing RNA (left) and siRNA (right) HeLa in the presence (bottom) or in the absence (top) of CD95/Fas treatment. Cell apoptosis was evaluated by staining with annexin V–FITC/propidium iodide. Values reported represent the percentage ± SD of positive cells obtained from three different experiments.

Piscataway, NJ) and immunoreactivity assessed by chemiluminescence reaction using the ECL Western detection system (Amersham Biosciences). Densitometric scanning analysis was performed by Mac OS X (Apple, Cupertino, CA) using ImageJ 1.62 software (National Institutes of Health, Bethesda, MD). The density of each band in the same gel was analyzed, values were summed, and then the percentage distribution across the gel was detected.

Immunoprecipitation experiments and ganglioside extraction

Briefly, crude mitochondria preparations obtained as described earlier were lysed in lysis buffer (10 mM Tris-HCl, pH 8.0, 150 mM NaCl, 1% Nonidet P-40, 1 mM PMSF, 10 mg of leupeptin/ml). After preclearing, the supernatant was immunoprecipitated with monoclonal anti-PrP mAb (SAF 32; SPI Bio) plus protein A–acrylic beads. A mouse IgG isotypic control (Sigma-Aldrich) was used.

The PrP^C immunoprecipitate was subjected to ganglioside extraction according to the method of Svennerholm and Fredman (1980), with minor modifications. Samples were normalized for protein content, determined as described earlier. Briefly, gangliosides were extracted twice in chloroform:methanol:water (4:8:3; vol/vol/vol) and subjected to Folch partition by the addition of water, resulting in a final chloroform:methanol:water ratio of 1:2:1.4. The upper phase, containing polar glycosphingolipids, was purified of salts and low–molecular weight contaminants using Bond Elut C18 columns (Superchrom, Milan, Italy), according to the method of Williams and McCluer (1980). The eluted glycosphingolipids were dried down and separated by high-performance thin-layer chromatography (HPTLC), using aluminum-backed silica gel 60 (20 × 20) HPTLC plates (Merck, Darmstadt, Germany). Chromatography was performed in chloroform:methanol:0.25% aqueous KCl (5:4:1; vol/vol/vol).

Plates were then immunostained for 1 h at room temperature with anti-GD3 mAb (Seikagaku, Chuo-ku, Tokyo, Japan) and then with HRP-conjugated anti–mouse IgM (Sigma-Aldrich). Immunoreactivity was assessed by chemiluminescence reaction using the ECL Western detection system (Amersham).

The immunoprecipitates were checked by Western blot, using the anti-PrP mAb (6H4; Prionics, Schlieren, Switzerland).

Flow cytometry analysis of crude mitochondria preparations

Crude mitochondria preparations, obtained as described, were fixed with 4% formaldehyde in PBS for 30 min at room temperature. After washings, mitochondria were incubated with specific antibodies to PrP mAb (SAF 32; SPI Bio)

for 1 h, washed again, and then incubated for 45 min with appropriate secondary antibodies conjugated with Alexa Fluor 488 (Molecular Probes). Samples were incubated at 4°C for 1 h and, after washing, they were labeled with anti-mouse Alexa Fluor 488 (Molecular Probes). After 45 min of incubation at 4°C, samples were washed and immediately analyzed on a cytometer. As negative and positive controls we used purified mitochondria incubated with mouse IgG1 immunoglobulin or with mAb to VDAC-1 (Santa Cruz Biotechnology), followed by an anti–mouse Alexa Fluor 488, respectively.

Swelling induction in mitochondria

Crude mitochondria preparations (0.5 mg protein/ml) were resuspended in SB (0.5 mg/ml) at the final volume of 1.5 ml. As a general rule, rec PrP was added 5 min after the recording was initiated. Total recording time was 25 min. As a positive control 300 mM Ca^{2+} was used, in order to induce protein transition pore opening and release of proteins (e.g., cyt C) that are normally stored in the intramembrane space. The mitochondrial membrane potential, $\Delta\Psi$, was quantified by cytofluorimetric analysis after mitochondria staining with 1 mM TMRM (Molecular Probes), a potentially sensitive probe. The incorporation of the dye TMRM was measured in the FL3 channel: low levels of TMRM incorporation (revealed by a decrease of red fluorescence) indicated a low $\Delta\Psi$, whereas high levels of TMRM incorporation (revealed by an increase of red fluorescence) indicated a high $\Delta\Psi$ (Rodolfo et al., 2004). We tested the effects on $\Delta\Psi$ after treatment with recombinant PrP for 20 min at different concentrations (from 0.1 to 1 μg/ml) either in the presence or absence of 10 μM Ca^{2+}. In parallel, the supernatants of swelling reactions of isolated mitochondria, carried out in the absence of TMRM, were examined by a commercial ELISA kit (R&D Systems, Minneapolis, MN) for cyt C detection. The cyt C release was quantified in all considered samples, including the positive control, and expressed as ng/ml.

Cell-death assay

Quantification of apoptosis was performed by evaluating DNA fragmentation in ethanol-fixed cells using propidium iodide (PI; Sigma-Aldrich). Alternatively, apoptosis was also quantified by flow cytometry after double staining using fluorescein isothiocyanate (FITC)–conjugated annexin V/PI apoptosis detection kit (Eppendorf, Milan, Italy), which allows discrimination among early apoptotic, late apoptotic, and necrotic cells.

Knockdown PrP^C by siRNA

CEM or HeLa cells were seeded (2×10^5 cells/ml) in a 60-mm dish in RPMI 1640–containing serum and antibiotics. Twenty-four hours after seeding, cells were transfected with 100 nM siRNA Hs PRNP (HP Genomewide siRNA Hs-PRNP-6; Qiagen, Valencia, CA), using HiPerFect Transfection Reagent (Qiagen), according to the manufacturer's instructions. As experimental control, cells were also transfected with 5 nM nonsilencing siRNA (AllStars Negative Control; Qiagen). After 72 h, cells were incubated with anti–CD95/Fas (250 ng/ml) for 1 and 2 h. Quantification of apoptosis was performed as reported. The transfection efficiency was evaluated by flow cytometry in cells transfected with a Qiagen positive silencing siRNA (FITC-siRNA). PrP^C expression was verified either by Western blot or flow cytometry analysis by using anti-PrP mAb (SAF 32).

Data analysis and statistics

All samples were analyzed with a FACScan cytometer (BD Biosciences, San Diego, CA) equipped with a 488-nm argon laser. At least 20,000 events were acquired. Data were recorded and statistically analyzed by a Macintosh computer using CellQuest software. The expression level of the analyzed proteins on isolated mitochondria was expressed as a median value of the fluorescence emission curve, and the statistical significance was calculated by using Student's t test or one-way variance analysis by using the Statview program for Macintosh. All data reported were verified in at least three different experiments and reported as mean ± SD. Only p values of <0.01 were considered as statistically significant.

REFERENCES

Anantharam V, Kanthasamy A, Choi CJ, Martin DP, Latchoumycandane C, Richt JA, Kanthasamy AG (2008). Opposing roles of prion protein in oxidative stress- and ER stress-induced apoptotic signaling. Free Radic Biol Med 45, 1530–1541.

Anderson HA, HiltBold EM, Roche PA (2000). Concentration of MHC class II molecules in lipid rafts facilitates antigen presentation. Nat Immunol 1, 156–162.

Aude-Garcia C, Villiers C, Candéias SM, Garrel C, Bertrand C, Collin V, Marche PN, Jouvin-Marche E (2011). Enhanced susceptibility of T lymphocytes to oxidative stress in the absence of the cellular prion protein. Cell Mol Life Sci 68, 687–696.

Ayllon V, Fleischer A, Cayla X, Garcìa A, Rebollo A (2002). Segregation of Bad from lipid rafts is implicated in the induction of apoptosis. J Immunol 168, 3387–3393.

Borchelt DR, Scott M, Taraboulos A, Stahl N, Prusiner SB (1990). Scrapie and cellular prion proteins differ in their kinetics of synthesis and topology in cultured cells. J Cell Biol 110, 743–752.

Bounhar Y, Zhang Y, Goodyer CG, LeBlanc AC (2001). Prion protein protects human neurons against Bax-mediated apoptosis. J Biol Chem 276, 39145–39149.

Brouckova A, Holada K (2009). Cellular prion protein in blood platelets associates with both lipid rafts and the cytoskeleton. Thromb Haemost 102, 966–974.

Campana V, Sarnataro D, Fasano C, Casanova P, Paladino S, Zurzolo D (2006). Detergent-resistant membrane domains but not the proteasome are involved in the misfolding of a PrP mutant retained in the endoplasmic reticulum. J Cell Sci 119, 433–442.

Chiesa R, Piccardo P, Dossena S, Nowoslawski L, Roth KA, Ghetti B, Harris DA (2005). Bax deletion prevents neuronal loss but not neurological symptoms in a transgenic model of inherited prion disease. Proc Natl Acad Sci USA 102, 238–243.

Choi CJ, Anantharam V, Saetveit NJ, Houk RS, Kanthasamy A, Kanthasamy AG (2007). Normal cellular prion protein protects against manganese-induced oxidative stress and apoptotic cell death. Toxicol Sci 98, 495–509.

Ciarlo L, Manganelli V, Garofalo T, Matarrese P, Tinari A, Misasi R, Malorni W, Sorice M (2010). Association of fission proteins with mitochondrial raft-like domains. Cell Death Differ 17, 1047–1058.

Csordas G, Renken C, Varnai P, Walter L, Weaver D, Buttle KF, Balla T, Mannella CA, Hajnoczky G (2006). Structural and functional features and significance of the physical linkage between ER and mitochondria. J Cell Biol 174, 915–921.

Degli Esposti M, Tour J, Ouasti S, Ivanova S, Matarrese P, Malorni W, Khosravi-Far R (2009). Fas death receptor enhances endocytic membrane traffic converging into the Golgi region. Mol Biol Cell 20, 600–615.

DeMarco ML, Dogget V (2009). Characterization of cell-surface prion protein relative to its recombinant analogue: insights from molecular dynamics simulations of diglycosylated, membrane-bound human prion protein. J Neurochem 109, 60–73.

Faitova J, Krekac D, Hrstka R, Vojtesek B (2006). Endoplasmic reticulum stress and apoptosis. Cell Mol Biol Lett 11, 488–505.

Foley GE, Lazarus H, Farber S, Uzman BG, Boone BA, McCarthy RE (1965). Continuous culture of human lymphoblasts from peripheral blood of a child with acute leukemia. Cancer 18, 522–529.

García-Ruiz C, Colell A, París R, Fernández-Checa JC (2000). Direct interaction of GD3 ganglioside with mitochondria generates reactive oxygen species followed by mitochondrial permeability transition, cytochrome c release, and caspase activation. FASEB J 14, 847–858.

García-Ruiz C, Colell A, Morales A, Calva M, Enrich C, Fernandez-Checa JC (2002). Trafficking of ganglioside GD3 to mitochondria by tumor necrosis factor-alpha. J Biol Chem 277, 36443–36448.

Garofalo T, Misasi R, Mattei V, Giammarioli AM, Malorni W, Pontieri GM, Pavan A, Sorice M (2003). Association of the death-inducing signaling complex with microdomains after triggering through CD95/Fas. Evidence for caspase-8-ganglioside interaction in T cells. J Biol Chem 278, 8309–8315.

Garofalo T, Giammarioli AM, Misasi R, Tinari A, Manganelli V, Gambardella L, Pavan A, Malorni W, Sorice M (2005). Lipid microdomains contribute to apoptosis-associated modifications of mitochondria in T cells. Cell Death Differ 12, 1378–1389.

Garofalo T, Tinari A, Matarrese P, Giammarioli AM, Manganelli V, Ciarlo L, Misasi R, Sorice M, Malorni W (2007). Do mitochondria act as "cargo boats" in the journey of GD3 to the nucleus during apoptosis? FEBS Lett 581, 3899–3903.

Gilady SY, Bui M, Lynes EM, Benson MD, Watts R, Vance JE, Simmen T (2010). Ero1α requires oxidizing and normoxic condition to localize to the mitochondria-associated membrane (MAM). Cell Stress Chaperones 15, 619–629.

Hachiya NS, Yamada M, Watanabe K, Jozuka A, Ohkubo T, Sano K, Takeuchi Y, Kozuca Y, SakaSegawa Y, Kaneko K (2005). Mitochondrial localization of cellular prion protein (PrPC) invokes neuronal apoptosis in aged transgenic mice overexpressing PrPC. Neurosci Lett 374, 98–103.

Hayashi T, Fujimoto M (2010). Detergent-resistant microdomains determine the localization of σ-1 receptors to the endoplasmic reticulum–mitochondria junction. Mol Pharmacol 77, 517–528.

Hu W, Kieseier B, Frohman E, Eagar TN, Rosenberg RN, Hartung HP, Stüve O (2008). Prion proteins: physiological functions and role in neurological disorders. J Neurol Sci 264, 1–8.

Hueber AO, Bernard AM, Herincs Z, Couzinet A, He HT (2002). An essential role for membrane rafts in the initiation of Fas/CD95-triggered cell death in mouse thymocytes. EMBO Rep 3, 190–196.

Jin S, Zhou F, Katirai F, Li PL (2011). Lipid raft redox signaling: molecular mechanisms in health and disease. Antioxid Redox Signal 15, 1043–1083.

Lai E, Teodoro T, Volchuk A (2007). Endoplasmic reticulum stress: signaling the unfolded protein response. Physiology (Bethesda) 22, 193–201.

Langlet C, Bernard AM, Drevot P, He HT (2000). Membrane rafts and signaling by the multichain immune recognition receptors. Curr Opin Immunol 12, 250–255.

Lewis V, Hooper NM (2011). The role of lipid rafts in prion protein biology. Front Biosci 16, 151–168.

Li XL, Wang GR, Jing YY, Pan MM, Dong CF, Zhou RM, Wang ZY, Shi Q, Gao C, Dong XP (2011). Cytosolic PrP induces apoptosis of cell by disrupting microtubule assembly. J Mol Neurosci 43, 316–325.

Malorni W, Garofalo T, Tinari A, Manganelli V, Misasi R, Sorice M (2008). Analyzing lipid raft dynamics during cell apoptosis. Methods Enzymol 442, 125–140.

Malorni W, Giammarioli A, Garofalo T, Sorice M (2007). Dynamics of lipid raft components during lymphocyte apoptosis: the paradigmatic role of GD3. Apoptosis 12, 941–949.

Masserini M, Palestini P, Pitto M (1999). Glycolipid-enriched caveolae and caveolae-like domains in the nervous system. J Neurochem 73, 1–11.

Matarrese P, Straface E, Palumbo G, Anselmi M, Gambardella L, Ascione B, Del Principe D, Malorni W (2009). Mitochondria regulate platelet metamorphosis induced by opsonized zymosan A-activation and long-term commitment to cell death. FEBS J 276, 845–856.

Mattei V, Garofalo T, Misasi R, Gizzi C, Mascellino MT, Dolo V, Pontieri GM, Sorice M, Pavan A (2002). Association of cellular prion protein with gangliosides in plasma membrane microdomains of neural and lymphocytic cells. Neurochem Res 27, 743–749.

Mattei V, Garofalo T, Misasi R, Circella A, Manganelli V, Lucania G, Pavan A, Sorice M (2004). Prion protein is a component of the multimolecular signaling complex involved in T cell activation. FEBS Lett 560, 14–18.

Mattei V, Barenco MG, Tasciotti V, Garofalo T, Longo A, Boller K, Löwer J, Misasi R, Montrasio F, Sorice M (2009). Paracrine diffusion of PrP(C) and propagation of prion infectivity by plasma membrane-derived microvesicles. PLoS One 4, e5057.

Mironov A Jr, Latawiec D, Wille H, Bouzamondo-Bernstein E, Legname G, Williamson RA, Burton D, DeArmond SJ, Prusiner SB, Peters PJ (2003). Cytosolic prion protein in neurons. J Neurosci 23, 7183–7193.

Naslavsky N, Shmeeda H, Friedlander G, Yanai A, Futerman HA, Barenholz Y, Taraboulos A (1999). Sphingolipid depletion increases formation of the scrapie prion protein in neuroblastoma cells infected with prions. J Biol Chem 274, 20763–20771.

Nieznanski K, Nieznanska H, Skowronek KJ, Osiecka KM, Stepkowski D (2005). Direct interaction between prion protein and tubulin. Biochem Biophys Res Commun 334, 403–411.

Petrakis S, Sklaviadis T (2006). Identification of proteins with high affinity for refolded and native PrPC. Proteomics 6, 6476–6484.

Prusiner SB (1998). Prions. Proc Natl Acad Sci USA 95, 13363–13383.

Rodolfo C, Mormone E, Matarrese P, Ciccosanti F, Farrace MG, Garofano E, Piredda L, Fimia GM, Malorni W, Piacentini M (2004). Tissue transglutaminase is a multifunctional BH3-only protein. J Biol Chem 279, 54783–54792.

Roucou X, Giannopulas PN, Zhang Y, Jodoin J, Goodyer CG, LeBlanc A (2005). Cellular prion protein inhibits proapoptotic Bax conformational change in human neurons and in breast carcinoma MCF-7 cells. Cell Death Differ 12, 783–795.

Siegel RM, Muppidi JR, Sarker M, Lobito A, Jen M, Martin D, Straus SE, Lenardo MJ (2004). SPOTS: signaling protein oligomeric transduction structures are early mediators of death receptor-induced apoptosis at the plasma membrane. J Cell Biol 167, 735–744.

Simons K, Ikonen E (1997). Functional rafts in cell membranes. Nature 387, 569–672.

Sorice M, Garofalo T, Misasi R, Manganelli V, Vona R, Malorni W (2011). Ganglioside GD3 as a raft component in cell death regulation. Anti Cancer Agents Med Chem May 9 [Epub ahead of print].

Sorice M et al. (2009). Raft component GD3 associates with tubulin following CD95/Fas ligation. FASEB J 23, 3298–3308.

Stahl N, Borchelt DR, Hsiao K, Prusiner SB (1987). Scrapie prion protein contains a phosphatidylinositol glycolipid. Cell 51, 229–240.

Stockinger W, Sailler B, Strasser V, Recheis B, Fasching D, Kahr L, Schneider WJ, Nimpf J (2002). The PX-domain protein SNX17 interacts with members of the LDL receptor family and modulates endocytosis of the LDL receptor. EMBO J 21, 4259–4267.

Svennerholm L, Fredman P (1980). A procedure for the quantitative isolation of brain gangliosides. Biochim Biophys Acta 617, 97–109.

Szegezdi E, Logue SE, Gorman AM, Samali A (2006). Mediators of endoplasmic reticulum stress-induced apoptosis. EMBO Rep 7, 880–885.

Taraboulos A, Scott M, Semenov A, Avrahami D, Laszlo L, Prusiner SB (1995). Cholesterol depletion and modification of COOH-terminal targeting sequence of the prion protein inhibit formation of the scrapie isoform. J Cell Biol 129, 121–132.

Vey M, Pilkuhn S, Wille H, Nixon R, DeArmond SJ, Smart EJ, Anderson RG, Taraboulos A, Prusiner SB (1996). Subcellular colocalization of the cellular and scrapie prion proteins in caveolae-like membranous domains. Proc Natl Acad Sci USA 93, 14945–14949.

Watt NT, Taylor DR, Gillott A, Thomas DA, Perera WS, Hooper NM (2005). Reactive oxygen species-mediated beta-cleavage of the prion protein in the cellular response to oxidative stress. J Biol Chem 280, 35914–35921.

Wieckowski MR, Giorgi C, Lebiedzinska M, Duszynski J, Pinton P (2009). Isolation of mitochondria-associated membranes and mitochondria from animal tissue and cells. Protocol 4, 1582–1590.

Williams MA, McCluer RH (1980). The use of Sep-Pak C18 cartridges during the isolation of gangliosides. J Neurochem 35, 266–269.

Williamson CD, Zhang A, Colberg-Poley AM (2011). The human cytomegalovirus protein UL37 exon 1 associates with internal lipid rafts. J Virol 85, 2100–2111.

Zamzami N, Maisse C, Métivier D, Kroemer G (2001). Measurement of membrane permeability and permeability transition of mitochondria. Methods Cell Biol 65, 147–158.

Zhang Y, Qin K, Wang J, Hung T, Zhao RY (2006). Dividing roles of prion protein in staurosporine-mediated apoptosis. Biochem Biophys Res Commun 349, 759–768.

Ziolkowski W, Szkatula M, Nurczyk A, Wakabayashi T, Kaczor JJ, Olek RA, Knap N, Antosiewicz J, Wieckowski MR, Wozniak M (2010). Methyl-beta-cyclodextrin induces mitochondrial cholesterol depletion and alters the mitochondrial structure and bioenergetics. FEBS Lett 584, 4606–4610.